A "standing-wave meter" to measure dispersion and loss of photonic-crystal waveguides

R. Wüest,[a] D. Erni, P. Strasser, F. Robin, and H. Jäckel
Electronics Laboratory, ETH Zurich, 8092 Zürich, Switzerland

B. C. Buchler, A. F. Koenderink, and V. Sandoghdar
Nano-Optics Group, Laboratory of Physical Chemistry, ETH Zurich, 8093 Zürich, Switzerland

R. Harbers
Laboratory for Electromagnetic Fields and Microwave Electronics, ETH Zurich, 8092 Zürich, Switzerland

(Received 11 August 2005; accepted 31 October 2005; published online 23 December 2005)

We demonstrate a "standing-wave meter" for measuring dispersion and loss along the length of a planar InP-based photonic-crystal waveguide. Light from a tunable cw laser was coupled into a single line-defect waveguide that terminated inside the crystal structure to form a retroreflector. This structure created a standing wave which was imaged using a scanning near-field optical microscope. By measuring the intensity distribution of the standing wave for a range of optical frequencies, waveguide dispersion and loss were measured with high accuracy. Comparisons of the measurement results with three-dimensional numerical simulations reveal that material dispersion effects as small as 0.8% affect the band structure measurably. © *2005 American Institute of Physics*. [DOI: 10.1063/1.2151254]

Planar photonic-crystal (PPC) devices lend themselves to a range of applications due to their compact light-guiding mechanism and highly tunable optical properties.[1] Examples include high-quality resonators with small mode volumes,[2] waveguides with radically reduced group velocities,[3] and miniaturized wavelength multiplexing devices.[4] Such structures often rely on the customizable dispersion relation of PPC defects. In order to make the best use of PPCs it would be very helpful to have a simple technique to measure dispersion and loss directly along the waveguide, thus avoiding the difficult analysis of optical input–output measurements which represent cumulative information along the whole path of light. Comparison with numerical modeling can then be used to determine the exact crystal parameters, predict the optical characteristics of other defect devices on the same chip, and characterize fabrication processes.[5] This is especially important for InP-based substrate-type PPC devices aimed at optoelectronic applications.

Previous work has demonstrated dispersion measurements using standard microscopy on the light scattered out of the structure.[6] In the case where the scattering is small or nonexistent, the method will fail. Scanning near-field optical microscopy (SNOM) has much to offer to photonic-device investigations[7] since it detects the evanescent field and is therefore not reliant on out-of-plane loss. Furthermore, the technique is not diffraction limited and can thus reveal the fine details of the light propagation in PPCs. An elegant combination of heterodyne interferometry and SNOM has been demonstrated on PPC waveguides.[8,9] The measured dispersion showed good qualitative agreement with numerical modeling. In our work we use a standard SNOM setup to measure the intensity of a standing wave formed by coupling light into a W1 waveguide (a single row of missing holes) which is terminated inside the PPC. Comparisons of the dispersion extracted from this "standing-wave meter" with three-dimensional (3D) numerical models show excellent agreement. In fact, we even observe a 0.8% variation in material dispersion intrinsic to the InP and InGaAsP materials from which our devices are made. The decay of the standing wave also allows an accurate determination of the waveguide loss when fitting the data with the appropriate analytical expression [Eq. (1)]. This method provides a representation of the underlying physics which is superior to a simple exponential fit to measured near-field intensities.[10]

The measurement setup depicted in Fig. 1(a) consists of a collection SNOM with an uncoated, sharp fiber tip.[7] Transverse-electrically (TE) polarized light from a tunable laser was coupled into the cleaved facet of a deeply etched trench access waveguide by an objective lens (NA=0.3). A large bend in the access waveguide ensures that the PPC is located away from the direct path of stray light coming from the incoupling region. To map the local electromagnetic field intensity, the tip is scanned along the sample surface. A tip–

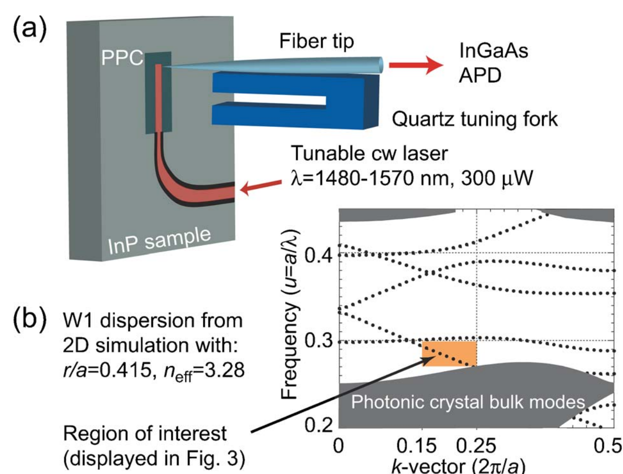

FIG. 1. (Color online) (a) SNOM setup in collection mode. (b) Dispersion relation of a W1 waveguide (2D simulation).

[a]Electronic mail: wueest@ife.ee.ethz.ch

 © 2005 American Institute of Physics
Downloaded 23 Dec 2005 to 129.132.223.246. Redistribution subject to AIP license or copyright, see http://apl.aip.org/apl/copyright.jsp

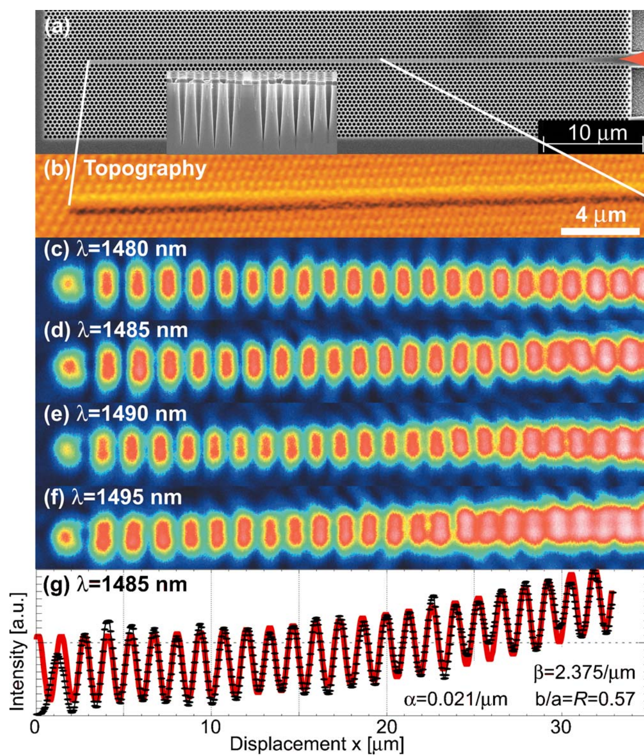

FIG. 2. (Color online) (a) SEM micrograph of the "standing-wave meter." The light is coupled in from the right-hand side. Inset: sample cross section with 3 μm deep holes. (b) SNOM topography data simultaneously acquired with (d). (c)–(f) SNOM optical data at several wavelengths. (g) Optical intensity of (d) along the waveguide (black symbols) and best fit of the electric-field intensity of a standing wave [solid thick line, see Eq. (1)] with the corresponding fit parameters.

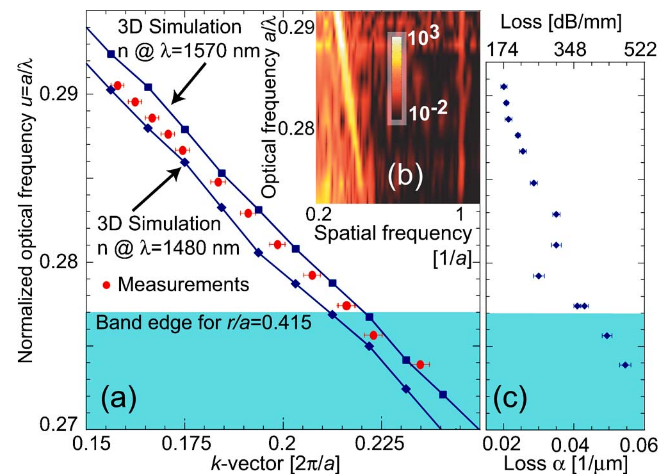

FIG. 3. (Color online) Region of interest marked in Fig. 1, showing waveguide dispersion and loss of the laterally even W1 mode: (a) measured k vectors from spatial FT peaks (filled circles) and k vectors simulated in three dimensions using material indices for $\lambda=1480$ nm (diamonds) and for $\lambda=1570$ nm (squares); (b) spatial FT of the optical data along the waveguide; (c) waveguide losses measured by fitting Eq. (1) to the optical intensity along the waveguide [see Fig. 2(g)].

surface distance of 10–20 nm is maintained with the help of a quartz tuning fork using shear force feedback. Radiation scattered by the tip is partially collected by the fiber itself and propagates to an InGaAs avalanche photo diode (APD) photon counting module. This way we simultaneously collect the topography (tip height) and optical signal of the PPC structure. The sample consists of a slab waveguide with a core of InGaAsP (400 nm, lattice matched to InP) and an upper InP cladding layer (200 nm). The refractive indices of the materials decrease from $n=3.45$ and 3.176 (InGaAsP, InP) at $\lambda=1480$ nm down to $n=3.423$ and 3.165 (InGaAsP, InP) at $\lambda=1570$ nm (Ref. 11). The vertical slab waveguide supports one TE mode. The PPC structure uses a triangular array of holes (depth=3 μm) with a lattice constant of $a=430$ nm. Details on the fabrication can be found elsewhere.[12,13] As indicated in the two-dimensional (2D) band-structure simulation[14] in Fig. 1(b), the structure exhibits a TE band gap for $u=a/\lambda=0.27-0.43$. For the frequency interval accessible with our laser system ($u=0.274-0.291$) we expect to excite the laterally even mode of the W1 waveguide. An image of the terminated waveguide that formed our "standing-wave meter" is shown in Fig. 2(a).

SNOM measurements were carried out by scanning an area of roughly 6×30 μm^2 along the waveguide. The fast scan direction was orthogonal to the waveguide. Typical topography (b) and optical data (c)–(f) can be seen in Fig. 2. The topography data resolves individual PPC holes, therefore allowing an accurate correlation between topography and optical information. The optical data exhibits a very clear signature of two counterpropagating attenuated electromagnetic waves which form a standing-wave pattern. It is interesting to note that the last optical maximum is located at the first hole after the waveguide end and exhibits a phase slip and hence a different shape compared to the other maxima along the waveguide. This is due to the local decay of the mode field within the proper PPC.

To extract the periodicity of the optical modulation, we take a line cross section of both the optical data along the waveguide and the topography signal parallel to the waveguide along the nearest row of crystal holes. The topography data is then used to calibrate distances in the optical data. This is critical since our piezoscanner has significant nonlinearity, as evidenced by the compression of the crystal lattice on the right-hand side of Fig. 2(b). A corrected line section of the optical data is shown in Fig. 2(g). The spatial Fourier-transform (FT) spectra for all measured frequencies are combined in the color plot of Fig. 3(b). The peak positions in the spatial FT spectrum correspond to 2β, where β is the propagation constant. We denote the normalized k vectors as $k=\beta a/2\pi$. Figure 3(b) shows a clearly resolved waveguide mode around a spatial frequency of $0.3/a$ for high optical frequencies. The waveguide mode decreases in strength as the optical frequency approaches the band edge. Also visible in this plot is a small peak in the spatial FT data at exactly $1/a$, which is due to the interference of the two Bloch modes located in the first (β) and the first negative ($\beta-K$) Brillouin zones ($K=2\pi/a$) (Ref. 15). The center of this peak varies by less than 1%, which validates our piezononlinearity calibration. Hence, we are confident that we can determine spatial frequencies in the optical signal with high accuracy. The extracted values for the k vectors of the waveguide mode are depicted in Fig. 3(a) with error bars of 1% (red points).

To assess the dispersion properties of the fabricated W1 waveguide we employ a 3D plane-wave simulation package.[14] The simulation of the W1 waveguide was performed with 16 plane waves per unit cell and a supercell measuring $1a\times 7a$ laterally and $10a$ vertically. Since we are interested in the light guided through the waveguide core, other modes had to be filtered out. Therefore only those

Downloaded 23 Dec 2005 to 129.132.223.246. Redistribution subject to AIP license or copyright, see http://apl.aip.org/apl/copyright.jsp

modes are displayed for which the energy preserved in the slab waveguide exceeds a certain threshold. The 3D simulations were performed for two sets of refractive indices corresponding to the material properties at $\lambda=1480$ and 1570 nm. For a fill ratio of $r/a=0.415$ we achieve a very good agreement between the measured and calculated dispersion relations. Furthermore, the systematic trend of measured k vectors from one simulation to the other conclusively reveals material dispersion effects on the band structure [see Fig. 3(a)]. We therefore have been able to isolate a variation of 0.8% in material dispersion by comparing measured k vectors with k vectors simulated in three dimensions using two sets of material indices.

To extract the loss amplitude coefficient α and the reflection coefficient $R=b/a$, we fit the optical intensity along the waveguide with an expression that represents the electric-field intensity of two counterpropagating, attenuated electromagnetic waves,

$$|E(x)|^2 = |a \cdot e^{(x-\phi)(\alpha+i\beta)} + b \cdot e^{-(x-\phi)(\alpha+i\beta)}|^2, \quad (1)$$

ϕ is a spatial phase and a, b are real amplitudes. The best fit to the optical intensity at $\lambda=1485$ nm can be seen in Fig. 2(g) together with the corresponding fit parameters. Over the whole wavelength range, extracted values for the amplitude reflection coefficient lie within $R=0.3-0.6$. Values for α are depicted in Fig. 3(c). Starting at high frequencies well inside the band gap we find a loss of $\alpha \approx 0.02/\mu$m. This corresponds to a waveguide loss of about 180 dB/mm. Although this is a factor of 2 higher than the lowest loss reported for this type of W1 waveguide,[16] it can be explained by the large size and slight conical shape of the air holes in our structure. As the frequency approaches the band edge, the loss inevitably increases. The location of the band edge was confirmed to be at $u=0.277$ (light blue area indicated in Fig. 3) with the help of a 3D simulation for the perfect crystal. Although this band edge accounts for a less reliable determination of α at the lowest frequencies, the fitting procedure indicates that the accuracy of the loss values is at worst 6%. Also below the band edge we find in Fig. 3(b) less pronounced FT peaks and multimode behavior of the waveguide due to the excitation of bulk crystal modes.

In conclusion, we have shown that SNOM measurements of standing-wave patterns in PPC waveguides provide a highly accurate means for determining both the dispersion and propagation loss. Fourier analysis or fitting of the real-space intensity patterns obtained on the W1 waveguides allowed us to extract loss and dispersion with an accuracy of 6% and 1%, respectively. In combination with 3D numerical simulations, the method is even sufficiently sensitive to reveal a 0.8% variation in material dispersion over a wavelength span of 90 nm. Measurements of such an accuracy enable the exact characterization of fabricated devices and may serve as a generic benchmark for models used in photonic-crystal simulations.

This work was carried out in the framework of the Network of Excellence ePIXnet, the Swiss National Science Foundation program NCCR Quantum Photonics, and the priority program SP 1113 of the Deutsche Forschungsgemeinschaft (DFG). The samples were fabricated in FIRST, the Center for Micro- and Nanoscale Science at ETH Zurich.

[1] *Photonic Crystals: Physics, Fabrication and Applications*, edited by K. Inoue and K. Ohtaka (Springer, Berlin, 2004).
[2] B. S. Song, S. Noda, T. Asano, and Y. Akahane, Nat. Mater. **4**, 207 (2005).
[3] M. Notomi, K. Yamada, A. Shinya, J. Takahashi, C. Takahashi, and I. Yokohama, Phys. Rev. Lett. **87**, 253902 (2001).
[4] H. Takano, B. S. Song, T. Asano, and S. Noda, Appl. Phys. Lett. **86**, 241101 (2005).
[5] P. Kramper, M. Kafesaki, C. M. Soukoulis, A. Birner, F. Müller, J. M. R. Wehrspohn, U. Gösele, and V. Sandoghdar, Opt. Lett. **29**, 174 (2003).
[6] M. Lončar, D. Nedeljković, T. P. Pearsall, J. Vučković, A. Scherer, S. Kuchinsky, and D. C. Allan, Appl. Phys. Lett. **80**, 1689 (2002).
[7] V. Sandoghdar, B. C. Buchler, P. Kramper, S. Götzinger, O. Benson, and M. Kafesaki, in *Photonic Crystals-Advances in Design, Fabrication, and Characterization*, edited by K. Busch, S. Lölkes, R. Wehrspohn, and H. Föll (Wiley, Weinheim, 2004), pp. 215–237.
[8] H. Gersen, T. J. Karle, R. J. P. Engelen, W. Bogaerts, J. P. Korterik, N. F. van Hulst, T. F. Krauss, and L. Kuipers, Phys. Rev. Lett. **94**, 073903 (2005).
[9] R. J. P. Engelen, T. J. Karle, H. Gersen, J. P. Korterik, T. F. Krauss, L. Kuipers, and N. F. van Hulst, Opt. Express **13**, 4457 (2005).
[10] V. S. Volkov, S. I. Bozhevolnyi, P. I. Borel, L. Frandsen, and M. Kristensen, Phys. Rev. B **72**, 035118 (2005).
[11] A. Afromowitz, Solid State Commun. **15**, 59 (1974).
[12] P. Strasser, R. Wüest, F. Robin, K. Rauscher, B. Wild, D. Erni, and H. Jäckel, in *Proceedings of the 17th International Conference on Indium Phosphide Related Materials*, edited by J. H. Marsh (IEEE, Piscataway, NJ, 2005).
[13] R. Wüest, P. Strasser, F. Robin, D. Erni, and H. Jäckel, J. Vac. Sci. Technol. B **23**, 3197 (2005).
[14] S. G. Johnson and J. D. Joannopoulos, Opt. Express **8**, 173 (2001).
[15] S. I. Bozhevolnyi, V. S. Volkov, T. Søndergaard, A. Boltasseva, P. I. Borel, and M. Kristensen, Phys. Rev. B **66**, 235204 (2002).
[16] A. Talneau, M. Mulot, S. Anand, S. Olivier, M. Agio, M. Kafesaki, and C. M. Soukoulis, Photonics Nanostruct. Fundam. Appl. **2**, 1 (2004).

Downloaded 23 Dec 2005 to 129.132.223.246. Redistribution subject to AIP license or copyright, see http://apl.aip.org/apl/copyright.jsp